

All-optical synaptic electrophysiology probes mechanism of ketamine-induced disinhibition

Linlin Z. Fan¹, Ralda Nehme^{2,3}, Yoav Adam¹, Eun Sun Jung⁴, Hao Wu¹, Kevin Eggan^{2,3}, Don B. Arnold⁴ and Adam E. Cohen^{1,5*}

Optical assays of synaptic strength could facilitate studies of neuronal transmission and its dysregulation in disease. Here we introduce a genetic toolbox for all-optical interrogation of synaptic electrophysiology (synOptopatch) via mutually exclusive expression of a channelrhodopsin actuator and an archaerhodopsin-derived voltage indicator. Optically induced activity in the channelrhodopsin-expressing neurons generated excitatory and inhibitory postsynaptic potentials that we optically resolved in reporter-expressing neurons. We further developed a yellow spine-targeted Ca²⁺ indicator to localize optogenetically triggered synaptic inputs. We demonstrated synOptopatch recordings in cultured rodent neurons and in acute rodent brain slice. In synOptopatch measurements of primary rodent cultures, acute ketamine administration suppressed disynaptic inhibitory feedbacks, mimicking the effect of this drug on network function in both rodents and humans. We localized this action of ketamine to excitatory synapses onto interneurons. These results establish an in vitro all-optical model of disynaptic disinhibition, a synaptic defect hypothesized in schizophrenia-associated psychosis.

Changes in synaptic strength underpin learning and memory, and are the mechanisms by which most neuropeptides¹ and neuromodulators² act and contribute to the pathogenesis of many disorders. For studies of synaptic transmission and plasticity, a rapid, reliable, and quantitative means to probe the strength of synapses in a neural circuit is desirable.

Such capabilities have remained elusive owing to the difficulty of performing simultaneous electrophysiological measurements on defined pairs of neurons. Moreover, whole-cell patch-clamp measurements can dialyze cellular components, possibly interfering with plasticity mechanisms³. It is also technically challenging to maintain patch-clamp connections long enough to probe long-term plasticity.

Pairing of optogenetic actuation with fluorescence imaging⁴ constitutes a suitable alternative. The technical challenges are to ensure that optogenetic stimuli are delivered only to the presynaptic cells, that readouts come only from the postsynaptic cells, and that there is no optical cross-talk between stimulus and readout wavelengths.

In the Optopatch technique⁵, cells coexpressed a blue-light-activated channelrhodopsin, CheRiff, and a red-light-excited voltage indicator, QuasAr. This technique enabled high-speed measurements of neuronal excitability in cultured neurons⁶, acute brain slices, and peripheral nerves *in vivo*⁷. However, because the actuator and reporter are coexpressed, it may be difficult to distinguish synaptically mediated potentials from spurious optical stimulation of postsynaptic neurites that crossed the stimulus zone⁸.

Here we describe an approach to achieve mutually exclusive expression of optogenetic actuators in presynaptic cells and voltage reporters in postsynaptic cells (synOptopatch). We further developed a spine-targeted yellow Ca²⁺ indicator, spine-jRGECO1a, which we combined with simultaneous synOptopatch measurements to probe the relation between synaptic Ca²⁺ and membrane voltage during sub- and supra-threshold activity. The synOptopatch

technique functioned in primary cultured neurons and in acute brain slice. We developed pharmacological and genetic techniques to specify the sub-type of the pre- and postsynaptic cells.

We used synOptopatch to explore *in vitro* the mechanism of action of ketamine, a nonspecific *N*-methyl-D-aspartate receptor (NMDAR) antagonist. In healthy subjects, acute administration of sub-anesthetic amounts of ketamine induced symptoms that mimicked both positive and negative symptoms of schizophrenia⁹. In rodents and in healthy humans, ketamine induced elevated hippocampal glutamate and cortical hyperexcitability^{10–13}. In acute brain slices, ketamine decreased excitatory postsynaptic potential (EPSP) amplitudes in pyramidal neurons¹⁴, as expected for an NMDAR blocker, but also decreased the amplitude of disynaptic inhibition¹⁵. The mechanism by which a blocker of excitatory neurotransmission enhances network excitability has not been conclusively established¹⁶.

We found that ketamine had a dramatic disinhibitory effect in cultured neuronal networks. Combinations of Optopatch and synOptopatch measurements established that the dominant action of ketamine was to block excitatory-to-inhibitory (E-to-I) synapses. These results demonstrate that synOptopatch can be used to dissect complex synaptically mediated phenomena.

Results

Cre-mediated mutually exclusive expression of QuasAr2 and CheRiff. To image membrane voltage we used QuasAr2-Citrine containing a triple repeat of the K_v2.1 membrane trafficking signal^{17,18}. When coexpressed with the channelrhodopsin CheRiff in cultured rat hippocampal neurons, this genetically encoded voltage indicator (GEVI) reported optically evoked action potentials with signal-to-noise ratios of 39 ± 3 in a 500-Hz bandwidth (*n* = 12 neurons; all statistics are mean ± s.e.m. unless otherwise specified), but targeted stimulation of individual cells sometimes caused spurious

¹Department of Chemistry and Chemical Biology, Harvard University, Cambridge, MA, USA. ²Department of Stem Cell and Regenerative Biology, Harvard University, Cambridge, MA, USA. ³Stanley Center for Psychiatric Research, The Broad Institute of Harvard and MIT, Cambridge, MA, USA. ⁴Department of Biology, Section of Molecular and Computational Biology, University of Southern California, Los Angeles, CA, USA. ⁵Howard Hughes Medical Institute, Harvard University, Cambridge, MA, USA. *e-mail: cohen@chemistry.harvard.edu

direct optical stimulation of dendrites in a putative postsynaptic cell (Supplementary Fig. 1).

We developed a system based on Cre-recombinase¹⁹ for mutually exclusive expression of CheRiff-CFP and QuasAr2-Citrine (Fig. 1a). Cre-on CheRiff-CFP comprised a double-floxed inverse ORF (DIO) flanked by parallel double *lox* (*loxP* and *lox2272*) sites²⁰. Cre-off QuasAr2-Citrine was flanked by a *lox* variant, *FAS*, which does not show cross-reactivity with *loxP* or *lox2272* sites²¹ (Fig. 1a, Supplementary Fig. 2). Cotransduction of DIO Cre-on CheRiff-CFP, *FAS* Cre-off QuasAr2-Citrine, and low-titer Cre virus led to mutually exclusive expression of the actuator and reporter (Fig. 1b). The complete set of synOptopatch constructs is described in Supplementary Table 1.

Titration of the Cre virus tuned the ratio of actuator- to reporter-expressing neurons, from 0.07 at a Cre titer of 0.1 multiplicity of infection (MOI) to 8.3 at a Cre titer of 10 MOI, allowing control of the relative sizes of the pre- and postsynaptic populations (Fig. 1c). We proceeded with a Cre titer of 1 MOI, corresponding to a 1.1/1 ratio of actuator- to reporter-expressing neurons. Mean expression levels per expressing neuron of the CheRiff-CFP and QuasAr2-Citrine depended on the titers of the corresponding lentiviruses, but did not depend on the titer of the Cre virus, which suggests that a single copy of the Cre virus per cell was probably sufficient to activate expression of all CheRiff genes and inactivate expression of all QuasAr2 genes (Supplementary Fig. 2g). In analysis of 324 neurons across a range of titers of each of the three constructs, we did not observe any cells coexpressing CheRiff-CFP and QuasAr2-Citrine, thus confirming the orthogonality of the gene expression system (Supplementary Fig. 2h).

SynOptopatch enables all-optical measures of synaptic transmission. We delivered wide-field flashes of blue light (488 nm, 20–120 mW cm⁻², 10 ms, repeated at 1 Hz) to evoke spikes in the CheRiff-expressing neurons. The blue illumination covered a circular area 280 μm in diameter, typically encompassing 2.6 ± 0.3 CheRiff-expressing neurons (*n* = 10 fields of view), although not every CheRiff-expressing neuron necessarily synapsed onto each postsynaptic cell. We recorded the postsynaptic responses in the QuasAr2-expressing neurons via red excitation (640 nm, 400 W cm⁻², 500 Hz frame rate) and near-infrared fluorescence. Simultaneous manual patch-clamp measurements provided ground truth on the postsynaptic potentials in *n* = 10 neurons (Fig. 1d).

We observed a variety of responses, including purely excitatory, purely inhibitory, and mixed excitatory and inhibitory postsynaptic potentials (PSPs), with close correspondence of the optical and electrical traces (Supplementary Fig. 3a,b) reflecting the linearity and speed (1.2-ms response time) of the QuasAr2 GEV1. The mean EPSP amplitude was 22 ± 10 mV (*n* = 6 neurons) and the mean inhibitory postsynaptic potential (IPSP) amplitude was -6 ± 2 mV (*n* = 4 neurons). The mean slope of the *F* versus *V* relation was 45% ± 6% Δ*F*/*F* per 100 mV, where the error represents the s.e. of a fit to *n* = 10 cells (Supplementary Fig. 3c). Shot noise and camera noise together contributed a mean noise of 0.8% Δ*F*/*F* (corresponding to 1.8 mV) in a 500-Hz bandwidth.

To test for optical cross-talk, we measured the effect of blue light on QuasAr2 in cultures not expressing a channelrhodopsin (Supplementary Fig. 3d–f). QuasAr2 did not generate detectable photocurrent under red light (400 W cm⁻²), blue light (120 mW cm⁻²), or both. The blue light led via direct QuasAr2 fluorescence to transients of ~1.5% Δ*F*/*F*, which were readily distinguished from true postsynaptic responses by their rapid rise and fall concurrent with the blue stimulus.

To test the long-term stability of the cultures, we optogenetically evoked and probed PSPs before and after a 2-h interval during which the sample sat on the microscope stage. We did not observe a systematic change in the PSP response (*n* = 14 neurons, peak timing,

P = 0.8, two-sided paired-sample *t*-test; area under the curve (AUC), *P* = 0.8, two-sided paired-sample *t*-test, Supplementary Fig. 3g). To test for photodamage, we illuminated a sample with continuous red light at 400 W cm⁻². The signal photobleached to 50% of initial intensity in 29 min, but we did not observe a change in the PSP waveform during a 30-min exposure (Supplementary Fig. 3h,i).

The synOptopatch technique enabled repeated measurements on the same cells over several days. Chronic incubation with gabazine (20 μM, 48 h) followed by wash-out led to a homeostatic increase in the ratio of inhibitory to excitatory PSPs (IPSP/EPSP amplitude, 0.080 ± 0.03 before gabazine versus 0.23 ± 0.05 after gabazine, *n* = 9 neurons, *P* = 0.04, two-sided paired-sample *t*-test), whereas control plates showed no significant change in PSP over 48 h (IPSP/EPSP amplitude, 0.091 ± 0.03 before versus 0.099 ± 0.01 after 48 h, *n* = 5 neurons, *P* = 0.76, two-sided paired-sample *t*-test, Supplementary Fig. 4).

The synOptopatch constructs reported EPSPs and spikes in human induced pluripotent stem cell (hiPSC)-derived neurons (Supplementary Fig. 5), although the signal-to-noise ratio was lower than in primary neurons owing to low expression of the optogenetic constructs, and further improvements will probably be required for use in disease-modeling applications.

Resolving presynaptic cell types with pharmacology. Considering the complexity of neural circuits, we sought to isolate specifically excitatory versus inhibitory signals. SynOptopatch measurements in *n* = 403 cultured rat hippocampal neurons revealed pure EPSPs in *n* = 301 neurons (75%), pure IPSPs in *n* = 17 neurons (4%), and a mixed excitatory and inhibitory response in *n* = 85 neurons (21%; Fig. 2a). The mixed responses were presumably due to coactivation of excitatory and inhibitory presynaptic neurons. Indeed, we occasionally observed postsynaptic responses with intermittent inhibitory components, indicative of stochastic activation of an inhibitory presynaptic neuron (Fig. 2b). Targeted stimulation of individual presynaptic neurons with patterned blue light resolved mixed postsynaptic responses into individual excitatory and inhibitory components, thus confirming the presence of multiple presynaptic neurons (Fig. 2c).

We sought a pharmacological means to isolate the contributions of distinct presynaptic cell types and postsynaptic receptors to the PSP. Picrotoxin (50 μM) eliminated the inhibitory components of the PSP (Fig. 2d), (2*R*)-amino-5-phosphonovaleric acid (AP5) (50 μM) eliminated the slow NMDAR-dependent part of the EPSP while preserving the fast α-amino-3-hydroxy-5-methyl-4-isoxazolepropionic acid receptor (AMPA)-dependent component (Fig. 2e), and 2,3-dihydroxy-6-nitro-7-sulfamoyl-benzo[*f*]quinoxaline (NBQX) (20 μM) eliminated both the fast and slow excitatory components (Fig. 2f). In neurons with mixed presynaptic inputs, sequential application of each of these three blockers isolated the respective contributions to the PSP (Fig. 2g).

We ascribed the suppression by NBQX—an AMPAR blocker—of the putative NMDAR-dependent slow component of the EPSP to the voltage-dependent Mg²⁺ block of NMDARs; that is, without AMPAR-mediated depolarization, the NMDARs did not activate. Optogenetic induction of presynaptic spikes in a medium containing 0 mM Mg²⁺, NBQX (20 μM), and picrotoxin (50 μM) restored the slow NMDAR component of the PSP, but not the fast AMPAR component, thus confirming this hypothesis (Supplementary Fig. 6). Although other blockers could be used to achieve finer segmentation of postsynaptic responses by receptor subtypes, the above examples demonstrate the broad flexibility of synOptopatch for dissecting mechanisms of synaptic transmission.

We next probed whether IPSPs were primarily driven by direct optogenetic stimulation of inhibitory neurons versus an E-to-I disynaptic mechanism (Fig. 2h). In cells that showed mixed excitatory and inhibitory PSPs, addition of 6-cyano-7-nitroquinoxaline-

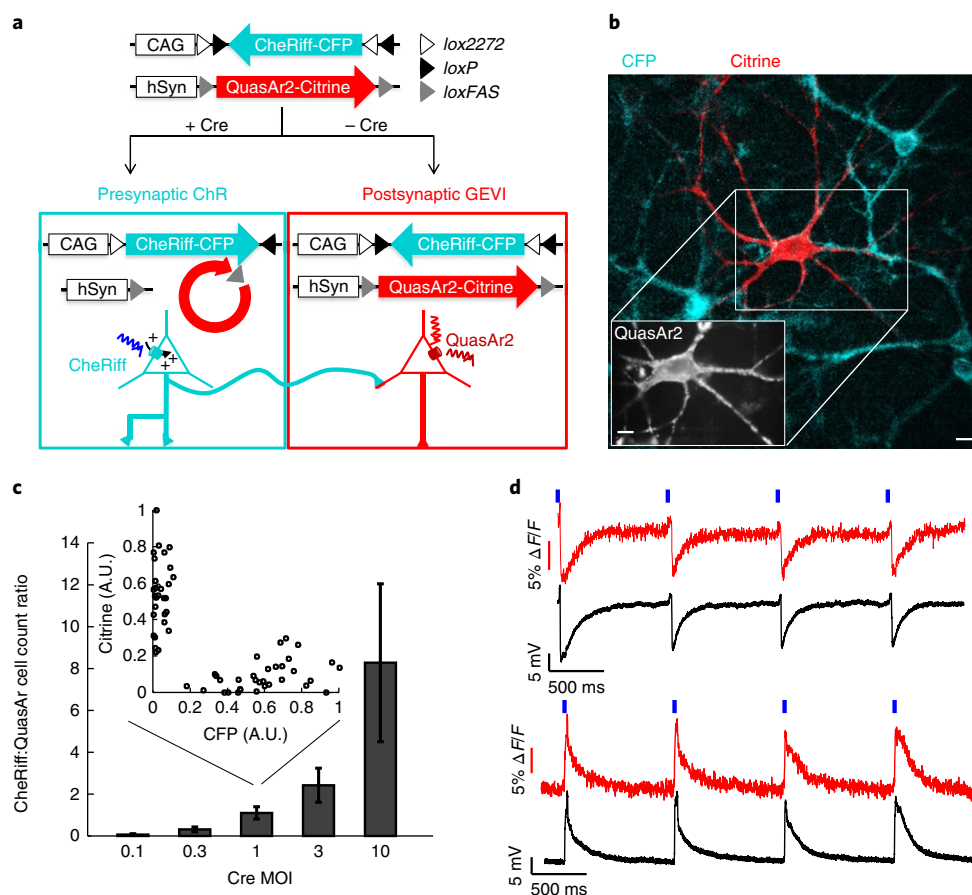


Fig. 1 | All-optical assay of synaptic function. **a**, Scheme for Cre-recombinase-mediated exclusive expression of Cre-on CheRiff and Cre-off QuasAr2. **b**, Cyan: presynaptic cell expressing CheRiff-CFP. Red: postsynaptic cell expressing QuasAr2-Citrine (Citrine fluorescence; inset shows QuasAr2 fluorescence). Scale bars, 10 μm . **c**, Ratio of cells expressing CheRiff to cells expressing QuasAr2 as a function of MOI of AAV virus encoding Cre. Error bars represent s.d. calculated via the bootstrap method. Inset: at MOI = 1, approximately equal numbers of neurons expressed CheRiff or QuasAr2, but no cells expressed both ($n = 63$ neurons). A.U., arbitrary units. **d**, Optical initiation and monitoring of primarily inhibitory (top) and primarily excitatory (bottom) postsynaptic potentials. These measurements were performed without synaptic blockers and may contain minor contributions from both excitatory and inhibitory inputs (for example, the slight uptick in the top recording). Blue, 10 ms of blue light stimulation; red, whole-cell single-trial unfiltered fluorescence; black, patch-clamp recording.

2,3-dione (CNQX) (20 μM), an AMPAR blocker, abolished both the excitatory and the inhibitory components of the PSP in eight of ten neurons tested, establishing that the IPSP was predominantly driven through a disynaptic (or polysynaptic) mechanism (Fig. 2h).

To measure purely monosynaptic PSPs, we adapted a protocol previously developed for optogenetic mapping of synaptic connections in brain slices²². Tetrodotoxin (TTX) (50 nM) blocked network activity; 4-aminopyridine (4-AP) (100 μM), a nonspecific potassium channel blocker, enabled the membrane potential to float; and gabazine (20 μM) blocked inhibitory signals. Optogenetic stimulation then evoked large monosynaptic EPSPs that were stable for > 1 h ($n = 12$ neurons; Fig. 2i).

Resolving active spines with spine-jRGECO1a. We next imaged spine-localized Ca^{2+} to probe the specific synapses activated during optogenetically induced synaptic transmission. GCaMP6s has previously been used to probe Ca^{2+} accumulation in individual synaptically activated dendritic spines under high-magnification imaging²³, but this indicator is not spectrally compatible with one-photon optogenetic stimulation. Although red-shifted Ca^{2+} indicators fulfill this requirement²⁴, under wide-field imaging conditions it was difficult to separate spine-specific signals from the much brighter background from the parent dendrite.

We therefore developed spine-enriched versions of the jRGECO1a²⁴ and GCaMP6s Ca^{2+} indicators. Dendritic spines contain high concentrations of filamentous actin, which has been used as a spine marker²⁵. The calponin homology domain of rat Utrophin (Utr; amino acids 1–261) binds to actin filaments²⁶, and at low concentration does not perturb their dynamics. We fused jRGECO1a and GCaMP6s to Utr and drove expression with a transcriptional regulatory system that used negative feedback to minimize levels of untargeted probe (Fig. 3a). High-resolution images showed that neurons expressing the complete construct had lower levels of dendritic background than did neurons expressing a construct lacking the transcriptional regulatory system (Supplementary Fig. 7)²⁷. Immunostaining for PSD-95 confirmed spine localization of the reporter (Supplementary Fig. 7). We compared the Ca^{2+} response of the jRGECO1a-Utr and cytosolic jRGECO1a in human embryonic kidney (HEK) cells. Ca^{2+} transients induced by the addition of ionomycin (10 μM) were indistinguishable between the two constructs ($\Delta F/F$ 1.6 ± 0.1 versus 1.5 ± 0.07 , $n = 26$ cells for jRGECO1a-Utr, $n = 29$ for cytosolic jRGECO1a, $P = 0.4$, Student's t -test) (Supplementary Fig. 7). For both the spine-jRGECO1a and spine-GCaMP6s indicators, we observed flickering patterns throughout the dendritic arbor, indicative of asynchronous activation of individual spines by synaptic inputs, as well as near-synchronous

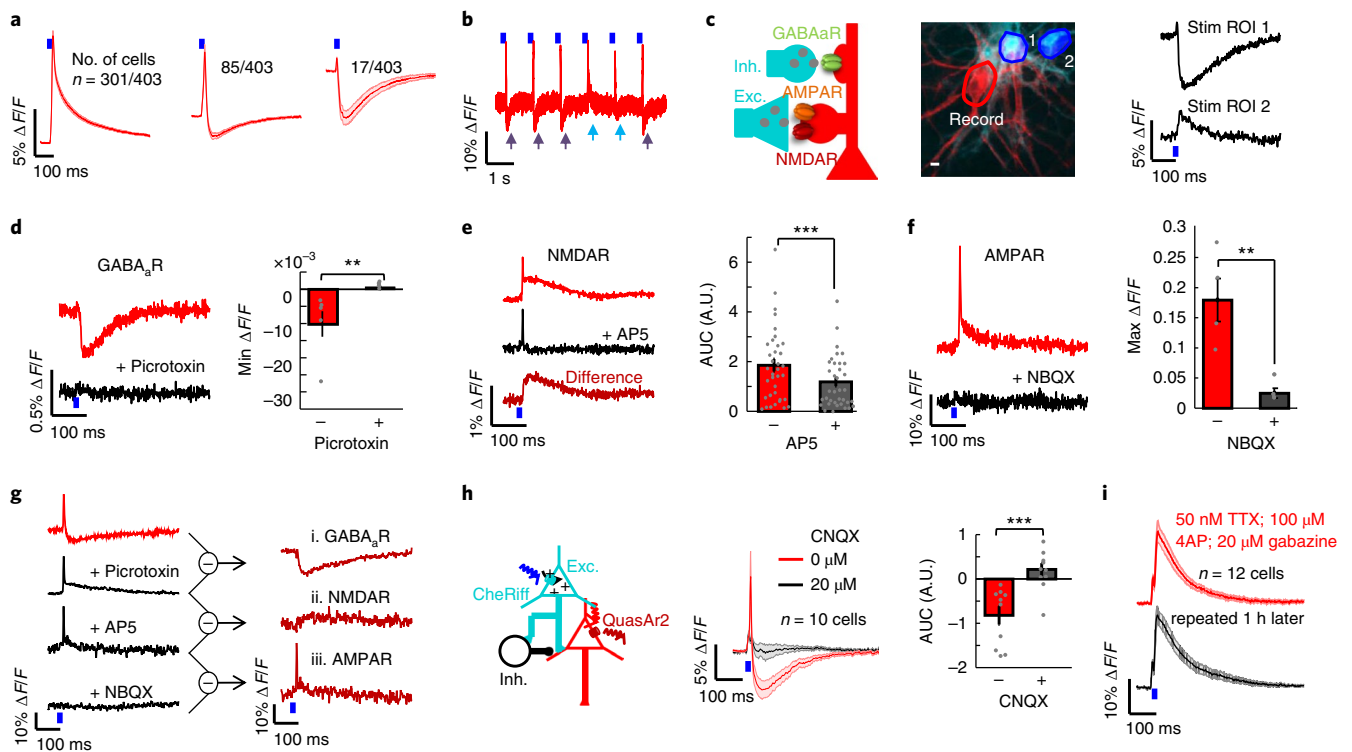


Fig. 2 | Pharmacological dissection of synaptic transmission and genetic tagging of inhibitory neurons. **a**, In the absence of drugs, cells showed purely excitatory, mixed excitatory and inhibitory, and purely inhibitory PSPs. **b**, Example single-cell single-trial trace showing intermittent optically evoked IPSPs (purple arrows) and IPSP failures (blue arrows). **c**, Left: schematic showing excitatory (Exc.) and inhibitory (Inh.) synaptic inputs into a single cell. Middle: cyan, CheRiff-CFP; red, QuasAr2-Citrine; blue, DMD masks for patterned blue light stimulation. Right: stimulation (Stim) of ROI 1 evoked a pure IPSP, and stimulation of ROI 2 evoked a pure EPSP. Two-trial average. Scale bar, 10 μm ($n=3$ times; representative data are shown). **d**, Optogenetically triggered EPSP (red) was blocked by picrotoxin (50 μM ; black; five-trial average). Bottom: quantification of minimum of $\Delta F/F$ before and after the addition of picrotoxin ($-0.99\% \pm 0.37\%$ versus $-0.02\% \pm 0.02\%$, $n=6$ neurons, $**P=0.04$, two-sided paired-sample *t*-test). **e**, NMDAR blocker AP5 (50 μM) blocked the slow component of EPSP (red, before; black, after AP5 addition; dark red, difference; five-trial average). Bottom: quantification of maximum of $\Delta F/F$ before and after the addition of NBQX and AP5 (1.86 ± 0.25 versus 1.19 ± 0.17 , $n=36$ neurons, $***P=2 \times 10^{-6}$, two-sided paired-sample *t*-test). **f**, AMPAR blocker NBQX (20 μM) blocked EPSPs (red, before; black, after NBQX addition; five-trial average). Bottom: quantification of maximum of $\Delta F/F$ before and after the addition of NBQX ($17.94\% \pm 3.58\%$ versus $2.48\% \pm 0.08\%$, $n=4$ neurons, $**P=0.035$, two-sided paired-sample *t*-test). **g**, Pharmacological dissection of a mixed EPSP and IPSP. The cell was recorded after sequential addition of picrotoxin (50 μM), AP5 (50 μM), and NBQX (20 μM). Five-trial average ($n=3$ times; representative data are shown). **h**, Left: schematic showing network inhibition. Middle: in cells with mixed excitatory/inhibitory PSPs, blockade of excitatory transmission with CNQX (20 μM ; black) relieved inhibition (red). Right: quantification of AUC before and after addition of CNQX (-0.80 ± 0.24 versus 0.19 ± 0.17 , $n=10$ neurons, $***P=0.001$, two-sided paired-sample *t*-test). **i**, 50 nM TTX, 100 μM 4-AP allowed detection of monosynaptic transmission (red). Signals were stable after 1 h under repeated measurements (black; $n=12$ neurons). All shaded error regions and error bars represent s.e.m.

activation of many spines by back-propagating action potentials (Supplementary Videos 1 and 2).

We then combined optogenetic stimulation of presynaptic inputs with simultaneous imaging of dendritic spine Ca^{2+} and somatic voltage. This measurement required several modifications to the synOptopatch constructs and to the optical setup. We developed a bicistronic construct to drive coexpression of spine-jRGECO1a and QuasAr2-dark Citrine⁵ (a nonfluorescent Citrine variant; Supplementary Fig. 8a). To minimize spurious activation of CheRiff by the yellow light used for jRGECO1a imaging, we fused CheRiff with a trafficking motif derived from $\text{K}_v2.1$, to localize expression to the soma²⁸, and we used a digital micromirror device to pattern the yellow illumination to span the dendritic arbor of the postsynaptic cell while avoiding presynaptic CheRiff-expressing somas (Fig. 3b). A dichroic beam splitter in the emission path separated the QuasAr2 from the spine-jRGECO1a emission, sending each to a separate camera (Supplementary Fig. 8b).

Wide-field blue light stimuli (488 nm, 200 mW cm^{-2} , 10-ms duration, repeated at 0.5 Hz) triggered presynaptic spikes, which in turn evoked somatic PSPs (detected with QuasAr2 fluorescence)

and synchronous Ca^{2+} transients in a subset of postsynaptic spines (Fig. 3b,c, Supplementary Fig. 9a,b). On average, we observed 8 ± 3 spines activated per stimulus (mean \pm s.d., $n=5$ neurons; Supplementary Fig. 9b). Occasionally, blue light stimulation triggered presynaptic action potentials, which led to brief spikes in QuasAr2 fluorescence and concurrent whole-cell Ca^{2+} transients (Fig. 3c,d, Supplementary Fig. 9a,b).

Simultaneous recording of spine Ca^{2+} and membrane voltage enabled detailed explorations of single-spine dynamics under both sub- and supra-threshold conditions. As expected, there was a positive correlation between the total synaptic Ca^{2+} transient and somatic PSP amplitude (Supplementary Fig. 9c, $n=14$ events, $R^2=0.42$, $P=0.01$). Because of the simultaneous activation of multiple spines it was not possible to apportion the PSP voltage to contributions from individual spines.

We next studied how the back-propagating action potentials (bAPs) modulated spine Ca^{2+} levels. We observed strong bAP-to-bAP correlation in the bAP-induced Ca^{2+} amplitude at the level of single spines (Fig. 3d, $R^2=0.66$, $n=100$ spines). Remarkably, a small portion of spines (4 of 100) did not exhibit Ca^{2+} transients

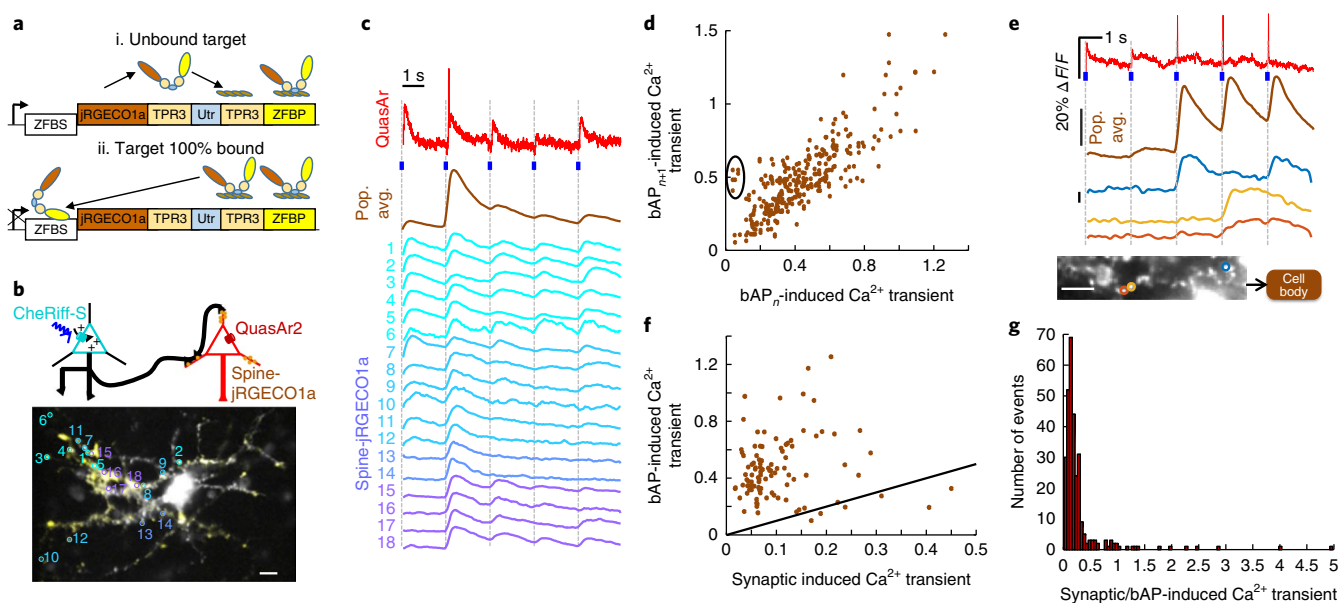


Fig. 3 | Simultaneous presynaptic optogenetic stimulation, spine Ca^{2+} imaging and somatic voltage imaging. **a**, Design of spine-targeted jRGECO1a. (i) TPR3 linkers⁴²: linked jRGECO1a, calponin homology domain of Utrophin (Utr), and a zinc finger DNA binding protein. (ii) Upon saturation of actin binding of spine-jRGECO1a, unbound protein accumulated in the nucleus, where it bound the zinc finger binding site downstream of the transcriptional start site and thereby blocked transcription. **b**, Top: schematic showing three-color imaging with blue-light-excitable soma-localized CheRiff in presynaptic cells, yellow-light-excitable spine-jRGECO1a, and red-light-excitable QuasAr2 coexpressed in postsynaptic cells. Bottom: spine-jRGECO1a channel overlaid with active spines colored in yellow. Active spines are circled and numbered with correspondingly colored traces in **c**. **c**, Blue: 10-ms blue light stimulation of soma-localized CheRiff. Red: QuasAr2 fluorescence. Orange: population average of spine-jRGECO1a fluorescence over all the spines. Cyan-purple: spine-jRGECO1a fluorescence in individual spines. Dashed lines mark stimulus times. **d**, Scatter plot of spine Ca^{2+} transients (ΔF) in pairs of successive bAPs. Transient amplitudes were predominantly correlated between events ($R^2=0.66$, $n=100$ spines, 3 bAPs), but some spines showed failures on some events (circled). **e**, bAP failure in spines. Blue: 10-ms blue light stimulation of soma-localized CheRiff. Red: QuasAr2 fluorescence. Orange: population average of spine-jRGECO1a over all the spines. Bottom: three spines on the same dendritic branch showed occasional bAP failures. **f**, Scatter plot of bAP-induced Ca^{2+} transients versus PSP-induced Ca^{2+} transients ($R^2=0.005$, $n=100$ spines). Black line indicates slope 1, corresponding to equal magnitude. **g**, Histogram of the ratio of Ca^{2+} transient amplitudes driven by bAPs versus synaptic events. All scale bars, 15 μm .

for some bAPs, while responding to others (Fig. 3e). Although the mechanism underlying these failures is not known, we can rule out bAP failure in the parent dendritic branches because we observed bAP activation of spines distal to spines with bAP failures (Fig. 3e, Supplementary Fig. 9d).

Finally, we studied the correlation between synaptically induced spine Ca^{2+} transients and bAP-induced transients. The correlation was much weaker than the bAP-to-bAP correlation ($R^2=0.005$, $n=100$ spines), presumably reflecting the different mechanisms driving synaptic and bAP spine Ca^{2+} transients (Fig. 3f). For a small fraction of spines (6 of 100) the synaptic Ca^{2+} transient exceeded the magnitude of the bAP transient, again possibly reflecting bAP failure in a subset of spines (Fig. 3f,g). These observations illustrate how the combination of synOptopatch with spine-jRGECO1a provides a platform for explorations of the interaction of voltage and calcium signals in single-spine dynamics.

SynOptopatch in acute brain slices. We next measured somatic PSPs in acute brain slices. To minimize nonspecific GEVI fluorescence from neuropil, we previously developed a somatically localized QuasAr variant with improved trafficking in vivo. This variant, QuasAr2s, reported action potentials in acute brain slices with a high signal-to-noise ratio¹⁷.

We validated synOptopatch in the visual cortex, using an Rbp4-Cre²⁹ driver to target expression of virally delivered Cre-on QuasAr2s-Citrine to a subset of L5 neurons. Cre-off CheRiff-CFP was expressed broadly, but not in the QuasAr2s-expressing neurons (Fig. 4).

To minimize the background fluorescence in the QuasAr channel, we patterned the red illumination with a digital micromirror

device (DMD) to illuminate expressing somas only¹⁷. Wide-field blue light stimulation (50 mW cm^{-2} , 5 ms, repeated at 1 Hz, 330 μm on a side) induced EPSPs, and sometimes spikes, which were readily detected on a single-trial basis (Fig. 4d). Addition of NBQX (10 μM) and 3-((R)-2-carboxypiperazin-4-yl)-propyl-1-phosphonic acid (CPP) (10 μM) eliminated the fluorescence transients in the QuasAr2-expressing cells, confirming that the signals were due to synaptic transmission (Fig. 4d,e).

Only one in 14 cells showed an IPSP, which was eliminated by gabazine (Fig. 4f). We hypothesized that the rarity of inhibitory signals arose because the reversal potential for Cl^- , the main ion transported by gamma-aminobutyric acid (GABA_A) receptors, was close to the resting potential in most cells. In patch-clamp measurements, the membrane potential and intracellular chloride concentration are typically set by the patch pipette to reveal inhibition³⁰. Lacking control of these parameters, we instead increased the extracellular K^+ concentration from 2.5 to 5 mM, raising the resting voltage by an estimated 14 mV³¹. Under high K^+ , NBQX (10 μM) and CPP (10 μM), blue light stimulation induced clear IPSPs in eight of ten cells (Fig. 4g, Supplementary Fig. 10). Of these responding cells, some (five of eight) also showed spontaneous activity, which was transiently suppressed by blue light stimulation. These results demonstrate the feasibility of all-optical assays for inhibitory transmission in acute brain slice.

SynOptopatch dissection of ketamine-induced disinhibition. We used the robust disinaptic inhibition in cultured networks (Fig. 2h) to explore the mechanism of ketamine-induced disinhibition. In cultured rat hippocampal neurons, we measured PSPs before and

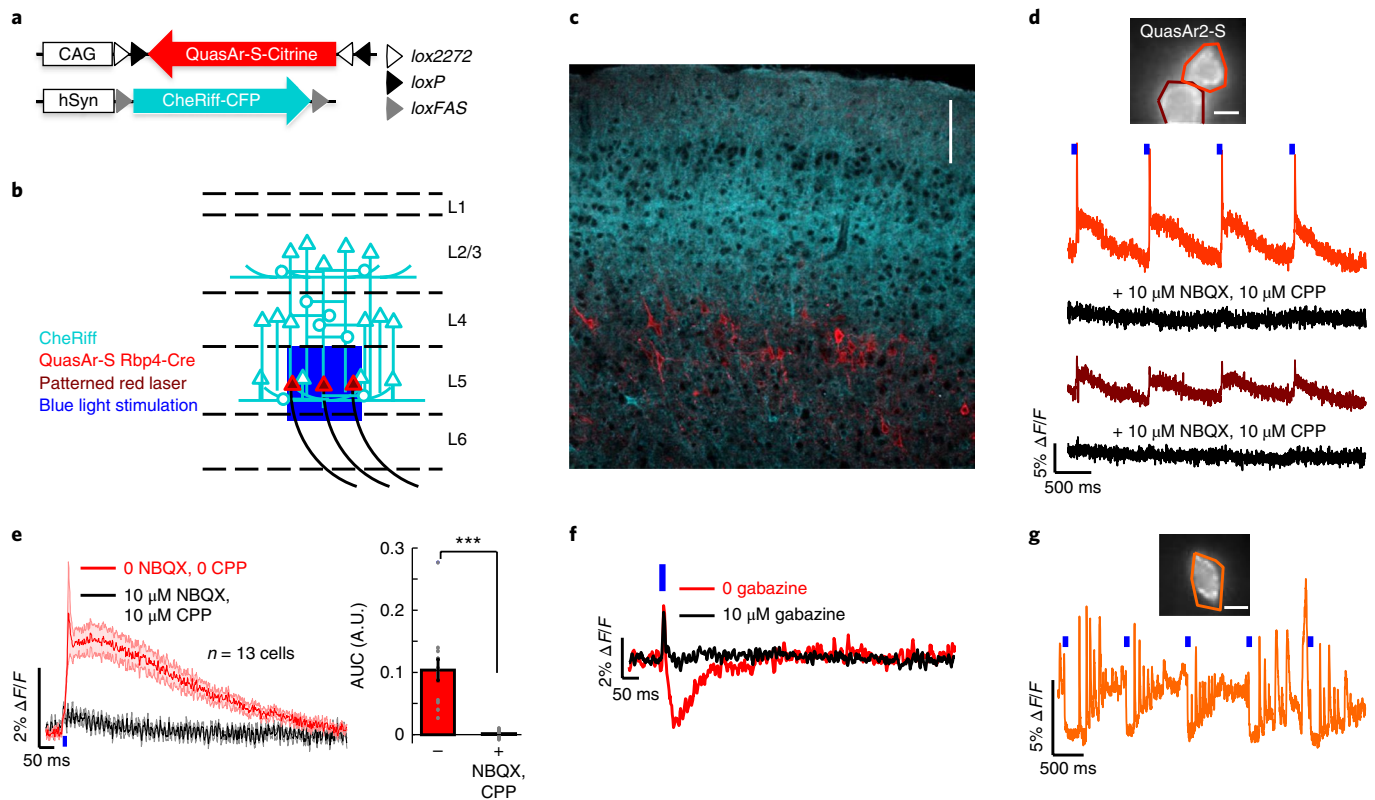


Fig. 4 | SynOptopatch detected EPSPs and IPSPs in acute mouse brain slice. a, b, Schematic showing the experimental design. Rbp4-Cre mice were injected with hSyn-Cre-off CheRiff-CFP and CAG-Cre-on soma-localized QuasAr (QuasAr-S; **a**), leading to QuasAr-S expression in layer 5 pyramidal neurons and CheRiff expression throughout the cortex (**b**). **c**, Confocal image of a fixed brain slice. Scale bar, 100 μm ($n=3$ times; representative data are shown). **d**, Top: fluorescence of QuasAr-S. Bottom: fluorescence traces of the two circled cells before (red) and after (black) addition of NBQX (10 μM) and CPP (10 μM) ($n=13$ cells; representative data are shown). **e**, Average PSPs of 13 cells before (red) and after NBQX and CPP (black). Shaded error bars, s.e.m. Right: quantification of AUC before and after addition of NBQX and CPP (0.1 ± 0.017 A.U. versus 0.002 ± 0.002 A.U., $n=13$ neurons, $***P=1 \times 10^{-4}$, two-sided paired-sample t -test). **f**, IPSP before (red) and after 10 μM gabazine (black). Five-trial average ($n=1$ in 14 cells). **g**, Single-trial IPSP detected under elevated (5 mM) extracellular K^+ and 10 μM NBQX, 10 μM AP5. Scale bars in **d, g**, 10 μm ($n=8$ cells; representative data are shown). All statistics are mean \pm s.e.m.

after applying 50 μM ketamine. For cells with purely excitatory inputs, ketamine suppressed the slow NMDAR component (AUC decreased from 1.08 ± 0.08 to 0.73 ± 0.05 A.U. (arbitrary units), $n=143$ neurons, $P=2 \times 10^{-6}$, two-tailed t -test; Fig. 5a,b), as expected for an NMDAR blocker. In cells with mixed excitatory and inhibitory inputs, ketamine largely abolished the IPSP (AUC increased from -6.1 ± 0.8 to 0.7 ± 1.2 A.U., $n=56$ neurons, $P=3 \times 10^{-6}$, two-tailed t -test; Fig. 5c,d). Thus acute ketamine administration in vitro largely suppressed inhibitory feedbacks, consistent with data from acute brain slices¹⁵.

We reasoned that ketamine-induced disinhibition could come from (1) blockade of E-to-I synapses, (2) decreased intrinsic excitability of inhibitory neurons, (3) increased excitability of excitatory neurons, or (4) blockade of I-to-E synapses (Fig. 5e). We conducted optogenetic experiments to test each hypothesis independently.

To determine the identity of the postsynaptic neurons we used an enhancer derived from the mouse *Dlx1* and *Dlx2* transcription factors, mI12b, to drive expression of eGFP in inhibitory neurons^{32–34}. We confirmed via immunostaining, Optopatch, and synOptopatch measurements that the enhancer drove expression in an inhibitory subpopulation (Supplementary Fig. 11)^{35,36}.

To study the effect of ketamine on monosynaptic excitatory transmission, we performed measurements in the presence of TTX and 4-AP (to block polysynaptic transmission) and gabazine (to block inhibitory transmission). We used mI12b-eGFP to distinguish postsynaptic responses in excitatory versus inhibitory

neurons and measured each postsynaptic cell before and after ketamine addition. Ketamine blocked E-to-I transmission significantly more strongly than E-to-E transmission, as measured by the slope of the plot of postsynaptic AUC after ketamine versus before ketamine (inhibitory postsynaptic neurons, slope, 0.32 ± 0.05 , $n=10$ neurons; excitatory postsynaptic neurons, slope, 0.52 ± 0.04 , $n=17$ neurons; analysis of covariance (ANCOVA) analysis of inhibitory versus excitatory postsynaptic neurons, $P=0.001$; Fig. 5f). These findings are consistent with the prevailing model that E-to-I transmission is a strong site of ketamine action.

To study the effect of ketamine on intrinsic excitability, we coexpressed CheRiff and QuasAr2-dark Citrine in the same cells (the Optopatch configuration), and used mI12b-eGFP to identify neuron subtypes. Under a wide variety of optogenetic stimulus patterns, ketamine did not significantly affect spike rate or action potential waveform in either inhibitory or excitatory neurons (Fig. 5g). Thus ketamine is unlikely to exert its disinhibitory effect by modulating the intrinsic excitability of either excitatory or inhibitory neurons.

To investigate the effects of ketamine on GABAergic synapses, we added NBQX and AP5 to block excitatory transmission. Regression fit showed that ketamine slightly but significantly increased the AUC of GABAergic synaptic transmission ($n=11$ neurons, $R^2=0.8$, $P=2 \times 10^{-4}$, F -test) (Fig. 5h), by slowing the kinetics of GABAergic synaptic transmission (Fig. 5i). This effect is consistent with prior observations in acute slice³⁷, but is of the wrong sign and too small to account for the overall disinhibitory effect of ketamine.

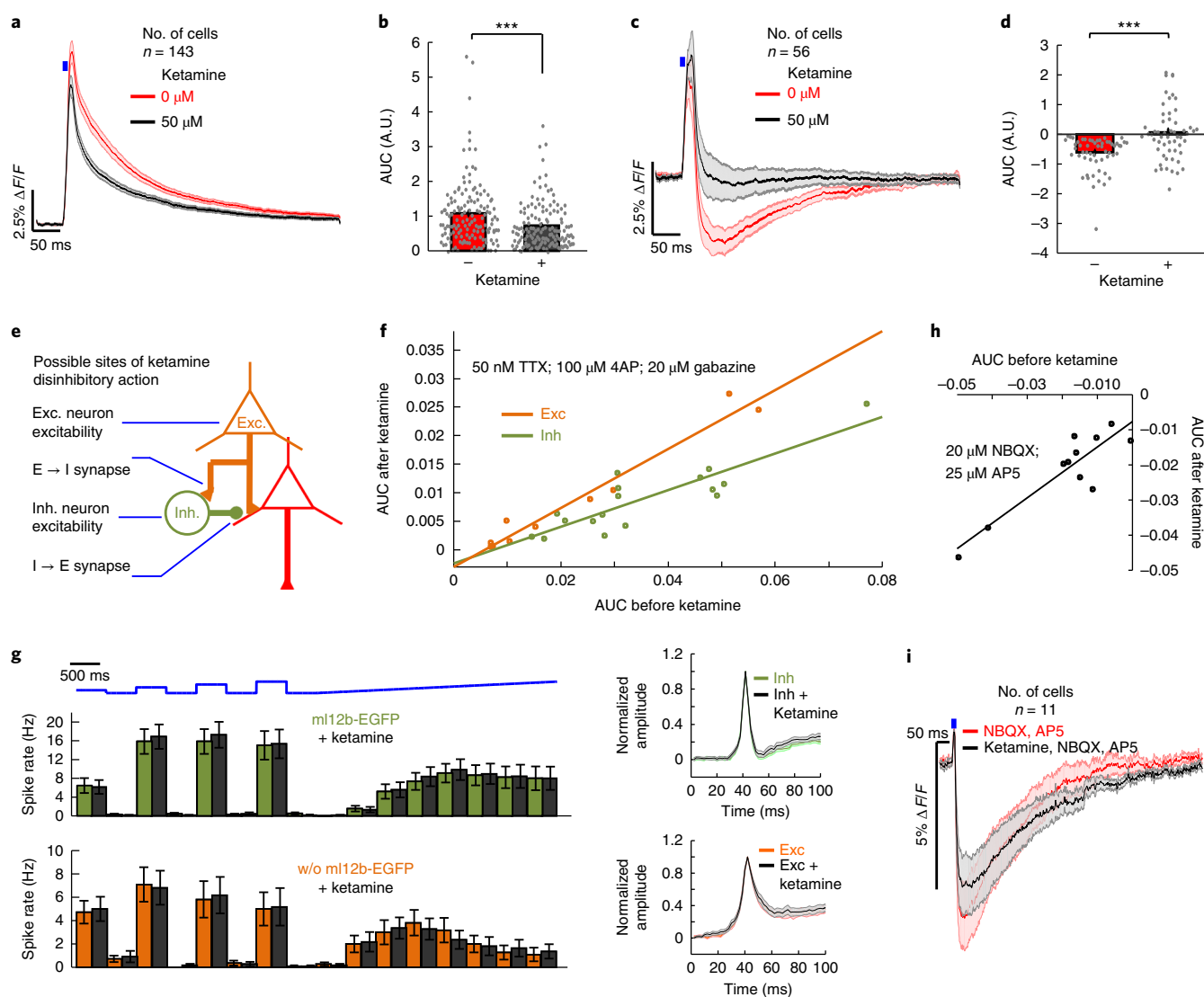


Fig. 5 | Mechanistic analysis of ketamine-induced disinhibition. **a**, For cells with pure EPSPs (red), ketamine (50 μM ; black) decreased the slow component of the EPSP ($n = 143$ neurons). **b**, Quantification of the AUC in **a** ($***P = 2 \times 10^{-6}$, two-tailed t -test). **c**, For cells with mixed EPSP and IPSP, the mean IPSP decreased after ketamine addition ($n = 56$ neurons). **d**, Quantification of AUC in **c** ($***P = 3 \times 10^{-6}$, two-tailed t -test). **e**, Possible sites of ketamine disinhibitory action: glutamatergic synapses onto inhibitory neurons; intrinsic excitability of excitatory or inhibitory neurons; GABAergic synapses. **f**, Under conditions of monosynaptic excitatory transmission (50 nM TTX, 100 μM 4-AP, 20 μM gabazine), ketamine (50 μM) induced a larger decrement in the EPSP in inhibitory neurons (green, $n = 17$ neurons) than in excitatory neurons (orange, $n = 10$ neurons). ANCOVA analysis comparing the slopes, $P = 0.001$. **g**, Left: in inhibitory neurons (green) the mean firing rate during a series of optogenetic stimuli was 12.9 ± 2.2 Hz before ketamine and 13.4 ± 2.2 Hz after ketamine ($n = 27$ neurons, $P = 0.86$). In excitatory neurons (orange) the mean firing rate was 5.1 ± 1.1 Hz before ketamine and 5.1 ± 1.1 Hz after ketamine ($n = 22$ neurons, $P = 0.98$). Right: in inhibitory neurons (green) the mean action potential width before ketamine was 6.9 ± 0.3 ms, and after ketamine it was 6.8 ± 0.3 ms ($n = 27$ neurons, $P = 0.81$, two-sided paired-sample t -test). In excitatory neurons (orange) the mean action potential width before ketamine was 9.3 ± 0.5 ms, and after ketamine it was 8.2 ± 0.8 ms ($n = 22$ neurons, $P = 0.30$, two-sided paired-sample t -test). **h**, Effect of ketamine on inhibitory transmission. IPSPs were probed in the presence of NBQX (20 μM) and AP5 (25 μM). Regression fit of AUC before and after ketamine of inhibitory synaptic transmission (slope = 0.72 ± 0.12 , $R^2 = 0.8$, $n = 11$ neurons). **i**, Red: IPSP before ketamine. Black: IPSP after ketamine. All shaded error regions and error bars, s.e.m. All statistics are mean \pm s.e.m.

Together, these results show that the disinhibitory action of ketamine is primarily via blockade of E-to-I transmission. More important, these results demonstrate a robust *in vitro* all-optical assay of disynaptic inhibition, a core circuit function that is hypothesized to be dysregulated in schizophrenia-associated psychosis¹⁶.

Discussion

The combined voltage and Ca^{2+} measurements revealed phenomena that merit further exploration. Although the mechanism of bAP

failure in dendritic spines is unknown, we speculate that this effect may arise in spines where the neck electrical resistance is large compared with the membrane resistance of the spine head, leading to significant attenuation of the bAP amplitude in the spine, and therefore failure to activate voltage-gated Ca^{2+} channels.

A specific action of ketamine on E-to-I synapses has been hypothesized¹⁶, but our experiments localize the disinhibitory effect to these synapses. Although parvalbumin interneurons express more NR2A and NR2C than do pyramidal neurons^{38,39},

heterologously expressed NMDAR subunits show little difference in ketamine sensitivity between subunits⁴⁰. Furthermore, the concentration of ketamine used in this study, 50 μ M, was far beyond the IC₅₀ reported for heterologously expressed NMDARs (0.5–0.7 μ M)⁴⁰. Thus the selectivity for E-to-I synapses probably comes from the fact that NMDARs contribute more to the EPSP in fast-spiking interneurons than in excitatory neurons⁴¹. These findings highlight the importance of measuring the functional effects of channel block in the neuronal context and not just on heterologously expressed channels.

We anticipate that the synOptopatch toolkit will be useful across a range of neuroscience applications, although some applications remain challenging. Direct measurements of spine voltage in primary neurons or acute slices will require improvements in sensitivity of the voltage indicator. Measurements of minis (PSPs induced by single vesicle releases) are also beyond the sensitivity of the existing indicators.

The acute slice measurements open the door to all-optical circuit mapping. In the present work, the GEVI expression was set by expression of the Cre recombinase, while the CheRiff expression was excluded from the Cre-expressing cells but not otherwise genetically targeted. A Cre-off-Flp-on GEVI combined with Cre-on-CheRiff would allow independent genetic specification of pre- and postsynaptic cell types. We expect that use of synOptopatch in vivo could open doors to the exploration of synaptic plasticity in learning and memory.

Online content

Any methods, additional references, Nature Research reporting summaries, source data, statements of data availability, and associated accession codes are available at <https://doi.org/10.1038/s41592-018-0142-8>.

Received: 20 December 2017; Accepted: 15 July 2018;

Published online: 1 October 2018

References

- van den Pol, A. N. Neuropeptide transmission in brain circuits. *Neuron* **76**, 98–115 (2012).
- Tritsch, N. X. & Sabatini, B. L. Dopaminergic modulation of synaptic transmission in cortex and striatum. *Neuron* **76**, 33–50 (2012).
- Kuner, T. & Augustine, G. J. A genetically encoded ratiometric indicator for chloride: capturing chloride transients in cultured hippocampal neurons. *Neuron* **27**, 447–459 (2000).
- Emiliani, V., Cohen, A. E., Deisseroth, K. & Häusser, M. All-optical interrogation of neural circuits. *J. Neurosci.* **35**, 13917–13926 (2015).
- Hochbaum, D. R. et al. All-optical electrophysiology in mammalian neurons using engineered microbial rhodopsins. *Nat. Methods* **11**, 825–833 (2014).
- Werley, C. A. et al. All-optical electrophysiology for disease modeling and pharmacological characterization of neurons. *Curr. Protoc. Pharmacol.* **78**, 11.20.1–11.20.24 (2017).
- Lou, S. et al. Genetically targeted all-optical electrophysiology with a transgenic Cre-dependent optopatch mouse. *J. Neurosci.* **36**, 11059–11073 (2016).
- Shemesh, O. A. et al. Temporally precise single-cell-resolution optogenetics. *Nat. Neurosci.* **20**, 1796–1806 (2017).
- Krystal, J. H. et al. Subanesthetic effects of the NMDA antagonist, ketamine, in humans: psychotomimetic, perceptual, cognitive, and neuroendocrine effects. *Arch. Gen. Psychiatry* **51**, 199–214 (1994).
- Kraguljac, N. et al. Ketamine modulates hippocampal neurochemistry and functional connectivity: a combined magnetic resonance spectroscopy and resting-state fMRI study in healthy volunteers. *Mol. Psychiatry* **22**, 562–569 (2017).
- Jackson, M. E., Homayoun, H. & Moghaddam, B. NMDA receptor hypofunction produces concomitant firing rate potentiation and burst activity reduction in the prefrontal cortex. *Proc. Natl. Acad. Sci. USA* **101**, 8467–8472 (2004).
- Di Lazzaro, V. et al. Ketamine increases human motor cortex excitability to transcranial magnetic stimulation. *J. Physiol.* **547**, 485–496 (2003).
- Hamm, J. P., Peterka, D. S., Gogos, J. A. & Yuste, R. Altered cortical ensembles in mouse models of schizophrenia. *Neuron* **94**, 153–167 (2017).
- Izumi, Y. & Zorumski, C. F. Metaplastic effects of subanesthetic ketamine on CA1 hippocampal function. *Neuropharmacology* **86**, 273–281 (2014).
- Grunze, H. C. R. et al. NMDA-dependent modulation of CA1 local circuit inhibition. *J. Neurosci.* **76**, 2034–2043 (1996).
- Lisman, J. E. et al. Circuit-based framework for understanding neurotransmitter and risk gene interactions in schizophrenia. *Trends Neurosci.* **31**, 234–242 (2008).
- Adam, Y. et al. All-optical electrophysiology reveals brain-state dependent changes in hippocampal subthreshold dynamics and excitability. *bioRxiv* Preprint at <https://doi.org/10.1101/281618> (2018).
- Gradinaru, V. et al. Molecular and cellular approaches for diversifying and extending optogenetics. *Cell* **141**, 154–165 (2010).
- Branda, C. S. & Dymecki, S. M. Talking about a revolution: the impact of site-specific recombinases on genetic analyses in mice. *Dev. Cell.* **6**, 7–28 (2004).
- Atasoy, D., Aponte, Y., Su, H. H. & Sternson, S. M. A FLEX switch targets Channelrhodopsin-2 to multiple cell types for imaging and long-range circuit mapping. *J. Neurosci.* **28**, 7025–7030 (2008).
- Saunders, A., Johnson, C. A. & Sabatini, B. L. Novel recombinant adeno-associated viruses for Cre activated and inactivated transgene expression in neurons. *Front. Neural Circuits* **6**, 47 (2012).
- Petreaun, L., Mao, T., Sternson, S. M. & Svoboda, K. The subcellular organization of neocortical excitatory connections. *Nature* **457**, 1142–1145 (2009).
- Chen, T.-W. et al. Ultrasensitive fluorescent proteins for imaging neuronal activity. *Nature* **499**, 295–300 (2013).
- Dana, H. et al. Sensitive red protein calcium indicators for imaging neural activity. *eLife* **5**, e12727 (2016).
- Fischer, M., Kaech, S., Knutti, D. & Matus, A. Rapid actin-based plasticity in dendritic spines. *Neuron* **20**, 847–854 (1998).
- Burkel, B. M., Von Dassow, G. & Bement, W. M. Versatile fluorescent probes for actin filaments based on the actin-binding domain of utrophin. *Cell Motil. Cytoskeleton* **64**, 822–832 (2007).
- Gross, G. et al. Recombinant probes for visualizing endogenous synaptic proteins in living neurons. *Neuron* **78**, 971–985 (2013).
- Baker, C. A., Elyada, Y. M., Parra-Martín, A. & Bolton, M. Cellular resolution circuit mapping in mouse brain with temporal-focused excitation of soma-targeted channelrhodopsin. *eLife* **5**, 1–15 (2016).
- Gerfen, C. R., Paletzki, R. & Heintz, N. GENSAT BAC cre-recombinase driver lines to study the functional organization of cerebral cortical and basal ganglia circuits. *Neuron* **80**, 1368–1383 (2013).
- Edwards, F. A., Konnerth, A. & Sakmann, B. Quantal analysis of inhibitory synaptic transmission in the dentate gyrus of rat hippocampal slices: a patch-clamp study. *J. Physiol.* **430**, 213–249 (1990).
- Dingledine, R. *Brain Slices* (Springer Science & Business Media, New York, 2013).
- Potter, G. B. et al. Generation of Cre-transgenic mice using Dlx1/Dlx2 enhancers and their characterization in GABAergic interneurons. *Mol. Cell. Neurosci.* **40**, 167–186 (2009).
- Poitras, L., Ghanem, N., Hatch, G. & Ekker, M. The proneural determinant MASH1 regulates forebrain Dlx1/2 expression through the I12b intergenic enhancer. *Development* **134**, 1755–1765 (2007).
- Colasante, G. et al. Rapid conversion of fibroblasts into functional forebrain GABAergic interneurons by direct genetic reprogramming. *Cell Stem Cell* **17**, 719–734 (2015).
- McCormick, D. A., Connors, B. W., Lighthall, J. W. & Prince, D. A. Comparative electrophysiology of pyramidal and sparsely spiny stellate neurons of the neocortex. *J. Neurophysiol.* **54**, 782–806 (1985).
- Kwan, A. C. & Dan, Y. Dissection of cortical microcircuits by single-neuron stimulation in vivo. *Curr. Biol.* **22**, 1459–1467 (2012).
- McNally, J. M., McCarley, R. W., McKenna, J. T., Yanagawa, Y. & Brown, R. E. Complex receptor mediation of acute ketamine application on in vitro gamma oscillations in mouse prefrontal cortex: modeling gamma band oscillation abnormalities in schizophrenia. *Neuroscience* **199**, 51–63 (2011).
- Kinney, J. W. A specific role for NR2A-containing NMDA receptors in the maintenance of parvalbumin and GAD67 immunoreactivity in cultured interneurons. *J. Neurosci.* **26**, 1604–1615 (2006).
- Xi, D., Keeler, B., Zhang, W., Houle, J. D. & Gao, W. J. NMDA receptor subunit expression in GABAergic interneurons in the prefrontal cortex: application of laser microdissection technique. *J. Neurosci. Methods* **176**, 172–181 (2009).
- Paoletti, P. & Neyton, J. NMDA receptor subunits: function and pharmacology. *Curr. Opin. Pharmacol.* **7**, 39–47 (2007).
- Jones, R. S. G. & Bühl, E. H. Basket-like interneurons in layer II of the entorhinal cortex exhibit a powerful NMDA-mediated synaptic excitation. *Neurosci. Lett.* **149**, 35–39 (1993).
- Klein, J. S., Jiang, S., Galimidi, R. P., Keefe, J. R. & Bjorkman, P. J. Design and characterization of structured protein linkers with differing flexibilities. *Protein Eng. Des. Sel.* **27**, 325–330 (2014).

Acknowledgements

We thank V. Joshi, K. Williams, M. Lee, and S. Begum for technical assistance. We thank V. Parot for help with analysis of spine Ca^{2+} data, S. Turney and the Harvard Center Brain Science (CBS) for loan of optical equipment, B. Sabatini (Harvard Medical School, Boston, MA, USA) for Rbp4-Cre mice, and C. Werley and L. Williams (Q-State Biosciences, Cambridge, MA, USA) for the mI12b plasmid. This work was supported by the Howard Hughes Medical Institute and a grant from the Gordon and Betty Moore Foundation. Y.A. was supported by a long-term fellowship from the Human Frontiers Science Program and by a postdoctoral fellowship from the Edmund and Lili Safra center for Brain Sciences. D.B.A. and E.S.J. were supported by NIH grant NS-089491. K.E. and R.N. were supported by the Stanley Center and NIMH grants (grant nos. 5U01MH105669-04 and 1U01MH115727-01).

Author contributions

L.Z.F. and A.E.C. conceived synOptopatch. L.Z.F. designed the synOptopatch and system, built the dual-view system, and acquired the optical electrophysiology data. L.Z.F. and A.E.C. analyzed the data and wrote the paper. L.Z.F., R.N., K.E., and A.E.C. designed the approach for implementation in human neurons. D.B.A., E.S.J.,

and L.Z.F. engineered spine-jRGECO1a. Y.A. created QuasAr2-Citrine, designed soma-localized QuasAr2 and CheRiff, and developed the brain slice imaging system. H.W. set up the patterned illumination system. All authors participated in revision of the manuscript.

Competing interests

A.E.C. and K.E. are founders of Q-State Biosciences. L.Z.F. and A.E.C. have filed a patent related to synOptopatch.

Additional information

Supplementary information is available for this paper at <https://doi.org/10.1038/s41592-018-0142-8>.

Reprints and permissions information is available at www.nature.com/reprints.

Correspondence and requests for materials should be addressed to A.E.C.

Publisher's note: Springer Nature remains neutral with regard to jurisdictional claims in published maps and institutional affiliations.

Methods

Design of synOptopatch. We tried several strategies for mutually exclusive expression of CheRiff and QuasAr2. We found that electroporation of two populations of neurons with QuasAr2 or CheRiff and mixed coculture led to insufficient survival of expressing neurons. We thus sought to take advantage of Cre-recombinase-controlled gene expression.

Cre-on constructs. Double lox sites *loxP* and *lox2272* were adopted from the vector pCAG-FLEX-fwd[Chrimson-tdT] (Addgene; 59137). The vector was linearized by double digestion with NheI and KpnI and purified by the GeneJET gel extraction kit (Fermentas). Inverted CheRiff-CFP cDNA was generated by PCR amplification and then combined with the pCAG-FLEX backbone by Gibson ligation. The FLEX-DIO-CheRiff-CFP construct was then amplified by PCR and cloned into a modified lentivirus backbone (Addgene; 51694), in which the original Ca²⁺/calmodulin-dependent protein kinase II (CaMKII) promoter was replaced by a chicken β -actin (CAG) promoter.

Cre-off constructs. We tried several strategies to create a Cre-off construct. We first created a Cre-off QuasAr2-Citrine by flanking forward QuasAr2-Citrine sequence with parallel double lox sites *loxP* and *lox2272*. Upon lentiviral delivery to cultured rat hippocampal neurons, either with or without coinfection with a Cre-expressing virus, the constructs individually showed the anticipated Cre-dependent expression (Supplementary Fig. 2a–c). We then used lentiviral vectors to coinfect neurons with both constructs, and delivered Cre virus at low MOI to activate CheRiff and inactivate QuasAr2 in a subset of the neurons. However, we observed many neurons that coexpressed actuator and reporter (Supplementary Fig. 2d,e).

We hypothesized that the coexpression might be due to the presence of *loxP* and *lox2272* sites in both Cre-on and Cre-off constructs, leading to Cre-mediated cross-reactions between the two constructs. We then turned to orthogonal FAS lox sites. FAS lox sites were adopted from the vector pAAV-Ef1a-FAS-ChETA-TdTomato-WPRE-pA (Addgene; 37089). The vector was linearized by double digestion with AscI and NheI enzymes and purified by the GeneJET gel extraction kit (Fermentas). QuasAr2-Citrine cDNA was generated by PCR amplification and combined with the Ef1a-FAS backbone via Gibson ligation. The sequence of FAS lox sites and QuasAr2 and Citrine was then amplified by PCR and cloned into a modified lentivirus backbone (Addgene; 51694), in which the original CaMKII promoter was replaced by a hSyn promoter.

When QuasAr2-Citrine was coexpressed with either m112b-EGFP or spine-jRGECO1a, the Citrine fluorescence had spectral overlap with the other fluorescent marker. We found that the presence of the Citrine tag was beneficial to trafficking. To keep the structural elements of the Citrine tag while eliminating its fluorescence, we mutated the Citrine chromophore from GYG to GGG using site-directed mutagenesis (Agilent) to create a dark Citrine construct.

Cre constructs. Cre cDNA segments were generated from the template of pCAG-Cre (Addgene; 13775) and cloned into a modified lentivirus backbone (Addgene; 51694) in which the original CaMKII promoter was replaced by an hSyn promoter.

Virus production, primary neuronal culture, and viral transduction.

Experiments in cultured neurons were primarily performed with homemade lentiviral vectors to facilitate rapid testing of many constructs. Experiments in acute brain slices were primarily performed with commercially produced AAV2/9 vectors.

Low-titer lentivirus production of synOptopatch. Plasmids encoding Cre-off QuasAr2-Citrine, Cre-off QuasAr2-dark Citrine, and Cre-on CheRiff-CFP were used to produce low-titer lentivirus according to published methods⁴³. Briefly, low-passage-number HEK293T cells (ATCC; CRL-11268) were plated onto gelatin-coated (Stemcell Technologies; 07903) 10-cm dishes. When HEK cells reached 80% confluence, the medium was exchanged to a serum-free Dulbecco's modified Eagle's medium (DMEM). After 0.5–1 h, cells were transfected using polyethylenimine (PEI; Sigma; 408727). 6.22 μ g of the vector plasmid, 4 μ g of the second-generation packaging plasmid psPAX2 (Addgene; 12260), and 1.78 μ g of viral entry protein VSV-G plasmid pMD2.G (Addgene; 12259) were mixed into 540 μ l of serum-free DMEM, and 16 μ l of 1 mg ml⁻¹ PEI were added in the end. The mixture was incubated at room temperature for 10 min and added dropwise to the plate. After 4 h, the medium was exchanged back to 10 ml of DMEM10. The supernatant was harvested at 36 h post-transfection, and another 10 ml of DMEM10 were added to the cells and incubated for another 24 h. At 60 h post-transfection, the supernatant was harvested again and combined with the first batch of supernatant, centrifuged for 5 min at 500g, and filtered through a 0.45- μ m filter (EMD Millipore; SE1M003M00). The unconcentrated virus was tested with Lenti-X GoStix (Clontech; 631243), aliquoted, and stored at -80 °C for neuronal transduction.

AAV Cre virus. High-titer AAV2/9 virus with hSyn Cre-GFP at a titer of 5.54×10^{13} genome copies (GC) ml⁻¹ was obtained from UPenn Vector Core. High-titer AAV2/9 virus with hSyn Cre at a titer of 2.30×10^{13} GC ml⁻¹ was obtained from the

Gene Transfer Vector Core at Massachusetts Eye and Ear Infirmary & Schepens Eye Research Institute (MEEI), Harvard Medical School.

Primary neuronal culture and viral transduction. All procedures involving animals were in accordance with the National Institutes of Health Guide for the care and use of laboratory animals and were approved by the Institutional Animal Care and Use Committee at Harvard University. Mouse experiments were performed on strain C57BL/6. Rat experiments were performed on strain Sprague Dawley.

Hippocampal neurons from P0 rat pups were dissected and cultured in NBActiv4 medium (Brainbits) at a density of 40,000 cm⁻² on glass-bottom dishes (InVitro Scientific) or pretreated dishes (Ibidi 81156) precoated with poly-D-lysine (Sigma P7205) and matrigel (BD Biosciences; 356234). At 2–4 h after plating, AAV or lenti Cre virus at MOI = 1 and Cre-on CheRiff-CFP low-titer lentivirus at MOI = 5 (typically 200 μ l) were added to the neurons. At 1 day in vitro (DIV), plating medium with virus was aspirated and glia cells were plated on top of the neurons at a density of 7,000 cm⁻². By DIV 5, glia had grown into a monolayer, and 2 μ M AraC was added into the neuronal culture medium to inhibit glial growth. At DIV 5–7, 1 ml of the culture medium was removed and saved for later use. Cre-off QuasAr2-Citrine low-titer lentivirus at MOI = 5 (typically 200 μ l) was added to the neurons: 24 h after the virus was added, the medium was replaced with the 1 ml of saved medium and 1 ml of fresh medium.

The titer of AAV or lenti Cre virus was determined by titration in neurons as shown in Supplementary Fig. 2c. The titer of low-titer lentivirus was evaluated by Lenti-X GoStix (Clontech).

Imaging and electrophysiology in primary neurons. Imaging apparatus

for primary neurons. Experiments were conducted on a home-built inverted fluorescence microscope equipped with 405 nm, 488 nm, 532 nm, 561 nm, 594 nm, and 640 nm laser lines and a scientific complementary metal-oxide semiconductor (CMOS) camera (Hamamatsu ORCA-Flash 4.0). Beams from lasers were combined using dichroic mirrors and sent through an acousto-optic tunable filter (Gooch and Housego TF525-250-6-3-GH18A) for temporal modulation of intensity of each wavelength. The beams were then expanded and sent either to a DMD (Vialux, V-7000 UV, 9515) for spatial modulation or sent directly into the microscope (to avoid power losses associated with the DMD). The beams were focused onto the back-focal plane of a 60 \times /1.2-NA (numerical aperture) water-immersion objective (Olympus UIS2 UPlanSApo \times 60/1.20 W, for primary neurons). For cyan fluorescent protein, Citrine, and QuasAr2, fluorescence emission was separated from laser excitation using a quad-band dichroic mirror (Semrock; D103-R405/488/532/635-t1-25 \times 36). Imaging of fluorescent proteins was performed at illumination intensities of 2–4 W cm⁻². Imaging of QuasAr2 direct fluorescence was performed at an illumination intensity of 400 W cm⁻². Stimulation of CheRiff was performed at an illumination intensity of 20–120 mW cm⁻².

The optimal camera frame rate entails a balance of signal-to-noise ratio (favoring a slower rate when camera electronic readout noise is significant), field of view (favoring a slower rate), and temporal resolution (favoring a faster rate). We found that at room temperature, all action potentials had a full-width at half-maximum > 5 ms, leading to an optimal frame rate of 500 Hz. For measurements at elevated temperatures one may need to image faster.

Imaging of primary culture. Measurements were performed on primary cultures at DIV 14–21. Experiments were conducted in extracellular solution (XC) containing 125 mM NaCl, 2.5 mM KCl, 3 mM CaCl₂, 1 mM MgCl₂, 15 mM HEPES, 30 mM glucose, pH 7.3, and adjusted to 305–310 mOsm with sucrose. Experiments were performed at 23 °C under ambient atmosphere.

For resolution of presynaptic cell types with pharmacology, synaptic blockers were added to the imaging medium. The blockers were NBQX (20 μ M; Tocris; 1044), CNQX (20 μ M; Tocris; 0190), D-AP5 (25 μ M; Tocris; 0106), gabazine (20 μ M; Tocris; SR-95531), and picrotoxin (50 μ M; Tocris; 1128). For probing of monosynaptic transmission, TTX (50 nM; Tocris; 1078) and 4-AP (100 μ M; Tocris; 0940) were added to the imaging medium.

To probe the effects of ketamine, we added 50 μ M ketamine (Zoetis) to the imaging medium.

Simultaneous electrophysiology recording and fluorescence imaging. Filamented glass micropipettes (WPI) were pulled to a tip resistance of 5–10 M Ω and filled with internal solution containing 125 mM potassium gluconate, 8 mM NaCl, 0.6 mM MgCl₂, 0.1 mM CaCl₂, 1 mM EGTA, 10 mM HEPES, 4 mM Mg-ATP, 0.4 mM Na-GTP, pH 7.3, adjusted to 295 mOsm with sucrose. Pipettes were positioned with a Sutter MP285 manipulator. Whole-cell current clamp recordings were acquired using a patch-clamp amplifier (A-M Systems, Model 2400), filtered at 5 kHz with the internal filter and digitized with a National Instruments PCIE-6323 acquisition board at 10 kHz.

Simultaneous whole-cell patch-clamp and fluorescence recordings were acquired on a home-built, inverted epifluorescence microscope, described above.

Immunostaining of m112b-labeled neurons. For experiments on primary culture, primary cultures were fixed and stained using primary mouse anti-Gad67

(Millipore; MAB5406) and secondary goat anti-mouse 594 (Abcam; ab150116) antibodies. The immunostaining followed a protocol described previously⁷.

Optopatch measurement of mI2b-labeled neurons. Neurons were transfected with lentivirus encoding Cre-off CheRiff-CFP, Cre-off QuasAr2-dark Citrine, and mI2b-EGFP.

Synaptic blockers (NBQX, D-AP5, and gabazine) were added to block network activity. Cells were stimulated with 500 ms of blue light (1 Hz) of increasing intensity (20–120 mW cm⁻²) for 4 s and ramp blue light of increasing intensity (0–120 mW cm⁻²) for another 4 s, while firing patterns were recorded under continuous red illumination.

Simultaneous imaging of postsynaptic spine-jRGECO1a and QuasAr2 with optogenetic presynaptic stimulation. Construction of a bicistronic construct with spine-jRGECO1a and QuasAr2. To avoid spectral overlap of spine-jRGECO1a and the Citrine tag of QuasAr2, we used QuasAr2-dark Citrine. We used the porcine teschovirus-1 (P2A) sequence to coexpress spine-jRGECO1a and QuasAr2-dark Citrine.

Gene delivery. Cre-on soma-localized CheRiff-CFP was lentivirally delivered to presynaptic cells, and the sparseness was controlled by the MOI of Cre virus (MOI = 0.5). The bicistronic construct with spine-jRGECO1a and QuasAr2-dark Citrine was delivered to neurons via calcium phosphate, as previously described⁵. Neurons expressing the reporters and not the actuator were selected for measurement.

Imaging apparatus. We modified the imaging apparatus for simultaneous spine-jRGECO1a and QuasAr2 imaging. We used a 40×/1.25-NA silicone oil Universal Plan Super Achromatic (UPLSAPO) objective (Olympus UIS2 UPLSAPO ×40/1.25). For cyan fluorescent protein, spine-jRGECO1a, and QuasAr2, fluorescence emission was separated from laser excitation using a quad-band dichroic mirror (Chroma; ZT405/488/561/640rpc). The 488-nm and 561-nm light were sent through the DMD (Vialux, V-7000 UV, 9515). Stimulation of soma-localized CheRiff was performed at an illumination intensity of 200 mW cm⁻². To image spine-jRGECO1a we used the DMD to pattern 561-nm light onto the postsynaptic cell while avoiding presynaptic CheRiff-expressing somata. The 561-nm light was at an intensity of 0.4 W cm⁻². Imaging of QuasAr2 direct fluorescence was performed with 640-nm light at an intensity of 400 W cm⁻².

A 640-nm dichroic beam splitter (Semrock; FF640-FDi01-25×36) in the emission path separated the QuasAr2 from the spine-jRGECO1a emission, sending each to a separate camera, an sCMOS camera (Hamamatsu ORCA-Flash 4.0) for voltage imaging and an EMCCD (electron-multiplying charge-coupled device) camera (Andor iXon^{EM+} DU-897E) for Ca²⁺ imaging (20 Hz).

Virus production, hiPSC-derived neuron culture, and viral transduction.

Concentrating synOptopatch lentivirus. Lenti-X concentrator (Clontech; 631231) was used to concentrate low-titer synOptopatch lentivirus. Concentrated lentivirus was then used for hiPSC-derived neuron experiments.

High-titer lentivirus encoding Cre. For experiments in hiPSC-derived neurons, high-titer lentivirus with Cre driven by an hSyn promoter was produced by Alstem LLC with a titer of 2.60×10^9 integral field units per milliliter.

hiPSC-derived neuron culture and viral transduction. To achieve orthogonal expression of actuator and reporter, we first tried lentiviral delivery of Cre-independent CheRiff and QuasAr2 to separate pools of hiPSCs in the stem cell state, followed by mixing and replating at the progenitor state. However, after 28 d of differentiation we detected only weak expression of both constructs, which was probably a consequence of gene silencing during differentiation. We then tried the Cre-dependent synOptopatch approach that had worked in primary neurons and achieved robust and non-overlapping expression of reporter and actuator (Supplementary Fig. 5g).

Neuronal differentiation of human stem cells was carried out as previously described⁴⁴, with the following modification. Human iPSCs with TetO-NGN2-PURO were plated onto plastic dishes. Doxycycline (2 μg ml⁻¹) was added at 1 d (DIV 1) after plating to induce NGN2 expression. Puro was added at DIV 2 to kill the cells that did not express NGN2. On DIV 4, differentiated neurons were replated at a density of 80,000 cm⁻² on preestablished rat glial monolayers grown on eight-well Ibidi dishes (80826) in neural basal medium with B27. On DIV 10, lentivirus of Cre at MOI = 1 was added into the medium and incubated for 1 d. On DIV 14, concentrated lentiviruses of Cre-on CheRiff and Cre-off QuasAr2 at MOI = 5 were added and incubated for 1 d. Fifty percent medium exchanges were done every 3–4 d. Two days before imaging, 200 nM all-trans-retinal was added to the medium.

Imaging in hiPSC-derived neurons. *Imaging apparatus for hiPSC-derived neurons.* We used the same imaging apparatus as for primary neurons, but a 40×/1.2-NA water-immersion objective (Zeiss C-apochromat ×40/1.2 W). Stimulation of CheRiff was performed at a higher illumination intensity of 400 mW cm⁻².

Imaging of hiPSC-derived neurons. For hiPSC-derived neurons, measurements were performed at DIV 30–42. Experiments were conducted in XC medium at 37°C controlled by a Tokai Hit stage top incubator (Tokai Hit, WSKM).

For potentiating synaptic transmission of hiPSC-derived neurons, cyclothiazide (CTZ) (50 μM; Tocris; 0713) was added to the imaging medium.

Virus production, acute brain slices, and viral injection. *AAV virus preparation.* FAS Cre-off CheRiff-CFP construct was cloned into an AAV vector, AAV2/9-hSyn-WPRE-SVPA, for custom AAV production. Cre-on soma-localized QuasAr2 was cloned into an AAV vector, AAV2/9-CAG-WPRE-SVPA, for custom AAV production.

All custom AAV production was by the Gene Transfer Vector Core at Massachusetts Eye and Ear Infirmary & Schepens Eye Research Institute (MEEI), Harvard Medical School.

Virus injection for acute slices measurement. AAV2/9 hSyn-Cre-off CheRiff-CFP (5.55×10^{13} GC ml⁻¹) and AAV2/9 CAG-FLEX QuasAr2S-Citrine (2.09×10^{12} GC ml⁻¹) were mixed in a 1/2 volume ratio for virus injection.

Rbp4-Cre^{+/−} mice were crossed with wild-type C57BL/6 mice. Pups were cryo-anesthetized at P0–P2 and immobilized dorsal side up under a stereotaxic microscope. Injections were made using home-pulled micropipettes (Sutter P1000 pipette puller), mounted in a microinjection pump (World Precision Instruments Nanoliter 2010) controlled by a microsyringe pump controller (World Precision Instruments Micro4). The micropipette was positioned using a stereotaxic instrument (Stoelting Digital Mouse Stereotaxic Instrument). Pups were injected in the left hemisphere, 0.9 mm lateral and 0.7 mm anterior to lambda. Starting at a depth of 0.6 mm beneath the surface of the skull, virus injections (40 nl, 5 nl s⁻¹) were performed at 0.1-mm increments as the pipette was withdrawn. Pups were placed back in their home cage once they were awake.

Genotyping. Genotyping for Rbp4 was performed with the PCR primer pairs: Cre 5': 5' TAT CTC ACG TAC TGA CGG TG 3' and Cre 3': 5' AGA CTA ATC GCC ATC TTC CAG C 3' to yield a 500-base-pair band from Cre.

Acute slice preparation. Acute brain slices were prepared from P16–P28 Rbp4-Cre^{+/−} mice. The mice were anesthetized by isoflurane and then perfused with carbogen (95% O₂, 5% CO₂)-saturated ice-cold slicing solution with the following composition (in mM): 110 choline chloride, 2.5 KCl, 1.25 NaH₂PO₄, 25 NaHCO₃, 25 glucose, 0.5 CaCl₂, 7 MgCl₂, 11.6 Na-ascorbate, and 3.1 Na-pyruvate. Mice were then decapitated and the brains were rapidly coronally sliced with 300-μm thickness on a vibratome (Leica; VT 1200S).

Slices were incubated for 45 min at 34°C in a carbogenated artificial cerebrospinal fluid (ACSF) with the following composition (in mM): 127 NaCl, 2.5 KCl, 1.25 NaH₂PO₄, 25 NaHCO₃, 25 glucose, 2 CaCl₂, and 1 MgCl₂. The osmolality of all solutions was adjusted to 300–310 mOsm and the pH was maintained at 7.3 under constant bubbling with carbogen.

Imaging in acute brain slices. *Imaging apparatus for acute slices.* Experiments were conducted on a home-built upright fluorescence microscope equipped with 488-nm and 640-nm laser lines and an sCMOS camera (Hamamatsu ORCA-Flash 4.0)¹⁷. Briefly, laser beams were combined using dichroic mirrors, sent through an acousto-optic tunable filter (Gooch and Housego; 48058-2.5-.55) for intensity modulation, and then expanded and focused onto the back-focal plane of a 20×/1.0-NA water-immersion objective (Olympus XLUMPLFLN ×20/1.0 W). Both 488-nm light and 640-nm light could go through an alternative optical path containing a digital micromirror device (Vialux, V-7000 UV, 9515) for patterned illumination: 640-nm light was patterned to illuminate only the somas of neurons, whereas 488-nm light was targeted to the whole field at an intensity of 50–100 mW cm⁻².

For fast data acquisition, a small field of view around the cell of interest was chosen at the center of the camera to achieve a frame rate of 500 frames per second.

Imaging acute slices. For acute slices, measurements were conducted in ACSF at 23°C under ambient atmosphere. The slice was immobilized in a Warner Instruments RC-27LD flow chamber using a slice anchor (Warner Instruments; SHD-27LH/2). ACSF, perfused with carbogen, was flowed through the chamber at a rate of 2 ml min⁻¹ and recycled through a flow pump (Fisher Scientific; 13-876-2).

To confirm that fluorescence transients arose from synaptic transmission, we added synaptic blockers to the imaging medium. The blockers were NBQX (10 μM; Tocris; 1044), (R)-CPP (10 μM; Tocris; 0247), and gabazine (10 μM; Tocris; SR-95531).

Confocal imaging. Acute slices were fixed and confocal fluorescence imaging was performed on an Olympus FV1000 confocal microscope at the Harvard Center for Brain Sciences microscope facility.

Data analysis. Data were analyzed with homemade code written in MATLAB.

Data analysis for primary culture. Fluorescence intensities from raw movies were extracted via a maximum likelihood pixel-weighting algorithm described in ref. ⁴⁵. Traces showing spontaneous spikes or PSPs were rejected (~5% of the data). The remaining traces were then averaged by alignment with each blue light stimulation.

We used several parameters to classify synaptic inputs. First, we calculated the AUC of the fluorescence trace corresponding to the PSP. Next we calculated the maximum height of the PSP (Amp). Cells that had AUC < 0 and Amp below the noise floor were classified as having purely inhibitory inputs; cells with AUC < 0 and Amp above the noise floor were classified as having mixed inputs; cells with AUC > 0 were classified as having purely excitatory inputs.

Data analysis for simultaneous spine Ca^{2+} and soma voltage recordings. Spines were identified by the amplitude of the fluorescence fluctuations at each pixel. A threshold was selected to identify up to 100 spines per neuron. Synaptically activated spines were identified by the following criteria: Ca^{2+} transients among the top 15% of all spines; above the noise level; and aligned with presynaptic stimulation. Fluorescence traces were corrected for photobleaching.

Data analysis for voltage recordings in hiPSC-derived neurons and acute brain slices. A region of interest comprising the cell body and adjacent neurites was manually defined, and fluorescence intensities were calculated from the unweighted mean of pixel values within the region of interest. Background fluorescence from a cell-free region was subtracted from the baseline fluorescence of the cell. Traces were then corrected for photobleaching and averaged by alignment with each blue light stimulation.

Statistics. All error ranges represent s.e.m., unless otherwise specified. For the same neurons before and after drug manipulation, paired-sample *t*-test was

used. For two-sample comparisons of a single variable, Student's *t*-test was used. Comparisons of ketamine effects on excitatory monosynaptic transmission for inhibitory versus excitatory postsynaptic neurons were made using a one-way analysis of variance. Analysis of ketamine effect on GABAergic synaptic transmission was made by linear regression fit. Probabilities of the null hypothesis $P < 0.05$ were judged to be statistically significant.

Reporting Summary. Further information on research design is available in the Nature Research Reporting Summary linked to this article.

Code availability. The custom MATLAB code is available from the corresponding author on reasonable request.

Data availability

The datasets generated and/or analyzed during the current study are available from the corresponding author on reasonable request. Add Gene numbers for constructs developed in this study are listed in Supplementary Table 1.

References

- Geraerts, M., Micheils, M., Baekelandt, V., Debyser, Z. & Gijssbers, R. Upscaling of lentiviral vector production by tangential flow filtration. *J. Gene Med.* **7**, 1299–1310 (2005).
- Nehme, A. R. et al. Combining NGN2 programming with developmental patterning generates human excitatory neurons with NMDAR-mediated synaptic transmission. *Cell Rep.* **23**, 2509–2523 (2018).
- Kralj, J. M., Douglass, A. D., Hochbaum, D. R., MacLaurin, D. & Cohen, A. E. Optical recording of action potentials in mammalian neurons using a microbial rhodopsin. *Nat. Methods* **9**, 90–95 (2012).

Life Sciences Reporting Summary

Nature Research wishes to improve the reproducibility of the work that we publish. This form is intended for publication with all accepted life science papers and provides structure for consistency and transparency in reporting. Every life science submission will use this form; some list items might not apply to an individual manuscript, but all fields must be completed for clarity.

For further information on the points included in this form, see [Reporting Life Sciences Research](#). For further information on Nature Research policies, including our [data availability policy](#), see [Authors & Referees](#) and the [Editorial Policy Checklist](#).

▶ Experimental design

1. Sample size

Describe how sample size was determined.

For each experiment, sample size was as large as could be practically achieved given the number of neurons available and the stability of the sample on the microscope. The number of independent rounds of neuronal culture was > 3 in each experiment, consistent with common practice. Sample size was determined to be adequate as follows:

Fig. 1c: Assuming a binomial distribution for number of Cre-expressing neurons (independent infection probabilities), sample size was selected so that different Cre MOIs would yield statistically significant differences in expression probability.
Figs 2d,e,f,h: Once the distribution of pre-drug and post-drug PSP waveforms was estimated from initial measurements, sample sizes were selected to be large enough to clearly resolve pre- and post-drug distributions with $> 95\%$ probability.
Figs 3d,f,g: The number of spines examined was sufficient to characterize the distribution of responses including sub-populations that represented $> 3\%$ of the overall spine population.

Fig. 4e: Once the distribution of pre-drug and post-drug PSP waveforms was estimated from initial measurements, sample sizes were selected to be large enough to clearly resolve pre- and post-drug distributions with $> 95\%$ probability.

Fig. 5a,b,c,d,f,g,h,i: Once the distribution of pre-drug and post-drug PSP waveforms was estimated from initial measurements, sample sizes were selected to be large enough to clearly resolve pre- and post-drug distributions with $> 95\%$ probability. For excitability measurements, sample sizes were sufficient to determine that ketamine did not affect any electrophysiological parameter by more than 5%.

Supplementary Figures

Fig. S2: Neuron populations were selected as in Fig. 1c.

Figs. S3c,f,h: Sample sizes were selected to yield $< 10\%$ relative error in extracted slopes.

Figs. S4c,d: Sample sizes were sufficient to detect chemically induced plasticity effects with $> 95\%$ confidence.

Fig. S6g: Sample size was sufficient to determine with $> 95\%$ confidence that the spine:dendrite fluorescence ratio was greater with the transcriptional feedback than without.

Fig. S6h: Sample size was sufficient to determine that any distance effects in spine brightness were $< 5\%$.

Fig. S6i: Sample size was sufficient to determine that any difference in fluorescence response of the spine-targeted vs. cytosolic jRGECO1a to a Ca^{++} transient were $< 5\%$.

Fig. S8c: Sample size was as large as possible. No statistical comparisons were made.

Fig. S10d,e,f: Sample size was sufficient to establish the differences between m12b+ and m12b- neurons with $> 95\%$ confidence.

Fig. S11e,f: Once the distribution of pre-drug and post-drug PSP waveforms was estimated from initial measurements, sample sizes were selected to be large enough to clearly resolve pre- and post-drug distributions with $> 95\%$ probability.

2. Data exclusions

Describe any data exclusions.

Neurons that showed spontaneous post-synaptic potentials or spontaneous spikes were excluded from the analysis. This criterion excluded < 10% of the data.

3. Replication

Describe whether the experimental findings were reliably reproduced.

All experiments were performed over at least three rounds of cell culture and were reliably reproduced.

4. Randomization

Describe how samples/organisms/participants were allocated into experimental groups.

Experiments on drug effects were performed on a randomly selected dish, and the same cells were measured before and after drug addition. This pre/post provided an internal control which minimized the effect of cell-to-cell and sample-to-sample variability. When internally controlled experiments were not possible (e.g. comparing excitatory vs. inhibitory neurons) measurements were performed on matched cultures prepared in parallel and randomly assigned to test conditions.

5. Blinding

Describe whether the investigators were blinded to group allocation during data collection and/or analysis.

Blinding was not practical since a single experimenter performed most cell culture, pharmacology, imaging, and data analysis. However, all measurements were performed with matched controls, across multiple rounds of cell culture, and generated quantitative data not subject to interpretive bias. Data analysis was performed in a batch mode, always treating experiment and control conditions in parallel.

Note: all studies involving animals and/or human research participants must disclose whether blinding and randomization were used.

6. Statistical parameters

For all figures and tables that use statistical methods, confirm that the following items are present in relevant figure legends (or in the Methods section if additional space is needed).

- | | |
|--------------------------|--|
| n/a | Confirmed |
| <input type="checkbox"/> | <input checked="" type="checkbox"/> The <u>exact sample size</u> (n) for each experimental group/condition, given as a discrete number and unit of measurement (animals, litters, cultures, etc.) |
| <input type="checkbox"/> | <input checked="" type="checkbox"/> A description of how samples were collected, noting whether measurements were taken from distinct samples or whether the same sample was measured repeatedly |
| <input type="checkbox"/> | <input checked="" type="checkbox"/> A statement indicating how many times each experiment was replicated |
| <input type="checkbox"/> | <input checked="" type="checkbox"/> The statistical test(s) used and whether they are one- or two-sided (note: only common tests should be described solely by name; more complex techniques should be described in the Methods section) |
| <input type="checkbox"/> | <input checked="" type="checkbox"/> A description of any assumptions or corrections, such as an adjustment for multiple comparisons |
| <input type="checkbox"/> | <input checked="" type="checkbox"/> The test results (e.g. P values) given as exact values whenever possible and with confidence intervals noted |
| <input type="checkbox"/> | <input checked="" type="checkbox"/> A clear description of statistics including <u>central tendency</u> (e.g. median, mean) and <u>variation</u> (e.g. standard deviation, interquartile range) |
| <input type="checkbox"/> | <input checked="" type="checkbox"/> Clearly defined error bars |

See the web collection on [statistics for biologists](#) for further resources and guidance.

► Software

Policy information about [availability of computer code](#)

7. Software

Describe the software used to analyze the data in this study.

All analysis was performed in Matlab. The code involved custom scripts written for the specifics of the datasets, but did not involve any novel algorithms.

For manuscripts utilizing custom algorithms or software that are central to the paper but not yet described in the published literature, software must be made available to editors and reviewers upon request. We strongly encourage code deposition in a community repository (e.g. GitHub). [Nature Methods guidance for providing algorithms and software for publication](#) provides further information on this topic.

► Materials and reagents

Policy information about [availability of materials](#)

8. Materials availability

Indicate whether there are restrictions on availability of unique materials or if these materials are only available for distribution by a for-profit company.

All plasmids created for the study are available on Addgene.

9. Antibodies

Describe the antibodies used and how they were validated for use in the system under study (i.e. assay and species).

Antibodies used included primary anti Gad67 (Millipore #MAB5406, dilution: 1:3000), anti GFP(Aves Labs Inc #GFP-1029, dilution: 1:10000), anti PSD95 (NeuroMab UC Davis #75-028, dilution: 1:1000), and secondary goat anti mouse 594 (Abcam #ab150116), goat anti chicken 488 (Life Technologies Alexa Fluor 488 #A11039), and goat anti mouse 594 (Life Technologies Alexa Fluor 594 #A11012) antibodies. These antibodies were validated in previous studies cited in the manuscript.

10. Eukaryotic cell lines

a. State the source of each eukaryotic cell line used.

Hek293T cell line, purchased from ATCC, was used in this study

b. Describe the method of cell line authentication used.

The cell line used in this study was not authenticated by our group

c. Report whether the cell lines were tested for mycoplasma contamination.

The cell line was tested negative for mycoplasma contamination

d. If any of the cell lines used are listed in the database of commonly misidentified cell lines maintained by [ICLAC](#), provide a scientific rationale for their use.

No commonly misidentified cell lines were used. Experiments were performed on primary neuron cultures, so confusion was not possible.

► Animals and human research participants

Policy information about [studies involving animals](#); when reporting animal research, follow the [ARRIVE guidelines](#)

11. Description of research animals

Provide details on animals and/or animal-derived materials used in the study.

Mouse experiments were performed on strain C57BL/6 of either sex (age: P16-P28). Rat experiments were performed on strain sprague dawley of either sex (age: P0).

Policy information about [studies involving human research participants](#)

12. Description of human research participants

Describe the covariate-relevant population characteristics of the human research participants.

The study did not involve human research participants.